ISSN 1990-7931, Russian Journal of Physical Chemistry B, 2026, Vol. 20, No. 2, pp. 150–161. © Pleiades Publishing, Ltd., 2026.
ISSN 1990-7931, Russian Journal of Physical Chemistry B, 2026. © Pleiades Publishing, Ltd., 2026.

Solvent Effects on the Structural and Electronic Properties of Triallyl Isocyanurate: Experimental and Theoretical Investigation

E. Taniş[a, *] (ORCID: 0000-0001-6815-9286), F. Akman[b] (ORCID: 0000-0001-5663-2021), U. Holikulov[c] (ORCID: 0000-0001-9144-5504), A. S. Kazachenko[d, e, f, g, **] (ORCID: 0000-0002-3121-1666), A. S. Kazachenko[f], N. Issaoui[h] (ORCID: 0000-0002-2350-7360), O. M. Al-Dossary[j] (ORCID: 0000-0002-5926-5500), and L. G. Bousiakou[k]

[a] *Department of Electrical Electronics Engineering, Faculty of Engineering and Architecture, Kırşehir Ahi Evran University, Kırşehir, 40100 Turkey*

[b] *Vocational School of Food, Agriculture and Livestock, University of Bingöl, Bingöl, 12000 Turkey*

[c] *Department of Optics and Spectroscopy, Samarkand State University, Samarkand, 140104 Uzbekistan*

[d] *Reshetnev Siberian State University of Science and Technology, Institute of Chemical Technologies, Krasnoyarsk, Russia*

[e] *Institute of Chemistry and Chemical Technology, Krasnoyarsk Scientific Center, Siberian Branch, Russian Academy of Sciences, Krasnoyarsk, 660036 Russia*

[f] *Siberian Federal University, Krasnoyarsk, 660041 Russia*

[g] *Voino-Yasenetsky Krasnoyarsk State Medical University of the Ministry of Healthcare of the Russian Federation, Krasnoyarsk, 660022 Russia*

[h] *Laboratory of Quantum and Statistical Physics (LR18ES18), Faculty of Sciences, University of Monastir, Monastir, 5019 Tunisia*

[j] *Department of Physics and Astronomy, College of Science, King Saud University, PO Box 2455, Riyadh, 11451 Saudi Arabia*

[k] *IMD Laboratories Co, R&D Section, Lefkippos Technology Park, NCSR Demokritos PO Box 60037, Athens, 15130 Greece*

**e-mail: eminetanis@ahievran.edu.tr*

***e-mail: leo_lion_leo@mail.ru, kazachenko.as@icct.krasn.ru*

Received March 1, 2025; revised October 16, 2025; accepted October 20, 2025

Abstract—This study explores the solvent effects on the structural, electronic, and vibrational properties of Triallyl Isocyanurate (TAIC) using a combined experimental and theoretical approach. Density Functional Theory (DFT) calculations at the B3LYP/6-311++G(d,p) level and experimental Fourier Transform Infrared (FT-IR) spectroscopy were employed to analyze the influence of different solvents (water, Tetrahydrofuran (THF), Dimethyl sulfoxide (DMSO), and acetonitrile (ACN)) on TAIC. The electronic properties of TAIC were examined through molecular electrostatic potential (MEP) and frontier molecular orbital (FMO) analyses, revealing an energy gap ranging from 4.8229 eV (THF) to 4.8366 eV (water). Ultraviolet-visible (UV-Vis) spectroscopy demonstrated that solvent interactions primarily affect absorption intensity rather than peak positions. To further investigate noncovalent interactions and electron density distribution, topological analyses, including Atoms in Molecules (AIM), Non-Covalent Interaction Reduced Density Gradient (NCI-RDG), and Electron Localization Function (ELF)-Localized Orbital Locator (LOL) analyses, were performed. AIM analysis confirmed the presence of hydrogen bonding in TAIC-solvent systems, with electron density and its Laplacian values at bond critical points (BCPs) ranging from 0.0085–0.0233 au (water), 0.0067–0.0106 au (THF), 0.0081–0.0104 au (DMSO), and 0.0043–0.0097 au (ACN). The hydrogen bond energies varied from −0.97 to −5.62 kcal/mol.

Keywords: triallyl isocyanurate, DFT, AIM, RDG, ELF-LOL

DOI: 10.1134/S1990793125701520

INTRODUCTION

Isocyanurate derivatives are actively used in materials science to obtain polymer composite materials with unique heat-resistant properties [1]. Isocyanurate polymer is known [2] to have a relatively strong molecular structure due to a combination of strong chemical bonds, ring structure, and high cross-link density, all of which contribute to greater rigidity than comparable polyurethanes.

Triallyl isocyanurate is an isocyanurate derivative. It is used as a cross linker for polyolefins, chlorinated

polyethylene, polyvinyl chloride, polymethyl methacrylate, peroxide crosslinking of ethylene propylene diene monomer rubber, nitrile butadiene rubbers, fluorinated elastomers and as an intramolecular plasticizer for styrene polymers. In the rubber industry it is used as an effective vulcanizer for rubbers and caoutchoucs. Improves physical and mechanical properties, elasticity, thermal stability and chemical stability. Scope of application: rubber goods, hoses, cable insulation, shoe soles and other polymer products [3–10]. In addition, TAIC can be used as an Efficient Electrolyte Additive [11].

The brominated form is sold as a fire retardant for olefin and styrene resins [12]. TAIC Provides heat and weather resistance, good dispersibility and high thermal stability (prevents yellowing) of products to which it is added [12]. Triallyl isocyanurate polymerized with methacrylate and divinylbenzene has been studied as a urea adsorbent in artificial kidneys [13]. Triallyl isocyanurate polymerized with vinyl acetate was used as a cross-linker in the synthesis of a chiral stationary phase for the separation of amino acid enantiomers using high performance liquid chromatography (HPLC) [14].

Theoretical studies of polymerization agents are important for understanding their energy structure and potential use [15].

Recently, theoretical research has paid special attention to the application of density functional theory (DFT) to study Nonlinear optics (NLO) materials. Thus, superalakalis [16–18], nanoclusters [19], supramolecular complexes [20] and others [21] are being actively studied. Theoretical studies of materials allow us to make assumptions about their possible characters and properties, which allows us to think through possible areas of their application.

The purpose of this work was Experimental and Theoretical Vibrational Spectroscopy investigtion, molecular electrostatic potential (MEP), Time-dependent density functional theory (TD-DFT) study, Atoms in Molecules (AIM), Non-Covalent Interaction Reduced Density Gradient (NCI-RDG), Electron Localization Function (ELF)-Localized Orbital Locator (LOL) analyses, the highest occupied molecular orbital (HOMO) and the lowest unoccupied molecular orbital (LUMO), chemical reactivity and NLO properties of triallyl isocyanurate.

MATERIALS AND METHODS

Experimental Details

1,3,5-Triallyl-1,3,5-triazine-2,4,6(1H,3H,5H)-trione, CAS Number:1025-15-6 was purchased from Sigma-Aldrich chemical company and used without purification. FT-IR spectra of TAIC and its various solutions were recorded using a Thermo Scientific Nicolet iS10 FTIR spectrophotometer. The measurements were performed in the range of 4000–400 cm^{-1} with a resolution of 4 cm^{-1} at room temperature. A total of 32 scans were accumulated for each spectrum to ensure a high signal-to-noise ratio. The spectra were recorded in ATR (Attenuated Total Reflectance) mode using a deuterated triglycine sulfate (DTGS) detector.

Computational Details

Theoretical calculations were performed using the Gaussian 09 [22] and GaussView 5.0 software packages [23], and by using Becke's three parameter exact exchange functional (B3) [24] and three parameter hybrid exchange functional with Lee–Yang–Parr correlation functional [25] method with 6-311++G(d,p) basis set. Firstly, ABCluster software [26] was used to generate initial structures of TAIC-solvent complexes. Initial guesses were checked to ensure that we obtained the true global minimum of each structure. Secondly, each of the generated structures was fully optimized at the DFT: B3LYP/6-311++G(d,p) level of theory determine the most stable geometry for each complex. Theroretical UV-Vis analysis was performed using TD-DFT/IEFPCM solvation method with 6-311++G(d,p) basis set. Multiwfn 3.8 program [27] was used for topological analyses and to draw electron localization function diagram (ELF), localized orbital locator (LOL) and atoms in molecules (AIM).

RESULTS AND DISCUSSIONS

Optimization of the molecular structure of the calculated compounds is the first important step for further calculations of physicochemical parameters [28]. The optimized Triallyl isocyanurate molecule is shown in Fig. 1.

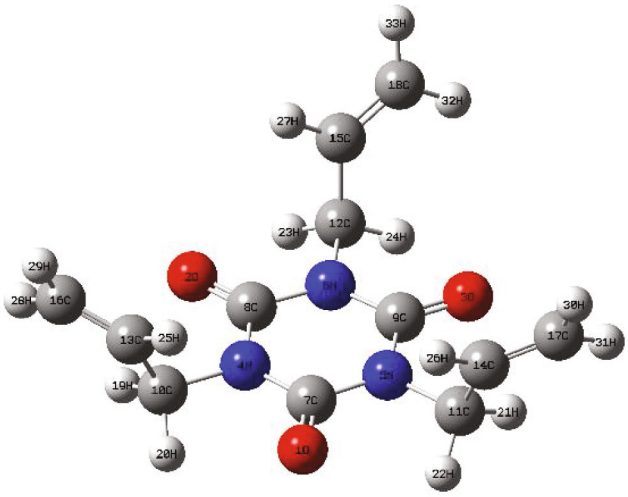

Fig. 1. The optimized Triallyl isocyanurate molecule.

Table 1. The selected important vibrational frequencies (cm^{-1}) determined theoretically (scaled by a factor of 0.9668) and experimentally for TAIC

in Water			in THF		
theoretical	experimental	assignments	theoretical	experimental	assignments
3108–2989	3720–2900	υC–H	3108–2988	3040–2780	υC–H
1720, 1635, 1632	1640	υC=O	1725–1641	1640	υC=O
1641	1630	υC=C	1647–1641	1640	υC=C
1389, 1195, 1078	1330, 1170	υC–N	1389, 1194, 1078	1460, 1360, 1190	υC–N
in DMSO			in ACN		
theoretical	experimental	assignments	theoretical	experimental	assignments
3108–2989	3020–2890	υC–H	3108–2989	3030–2850	υC–H
1720–1633	1660	υC=O	1720–1634	1550–1330	υC=O
1642–1633	1660	υC=C	1642–1634	1550	υC=C
1389, 1195, 1078	1430, 1310, 1050	υC–N	1389, 1195, 1078	1330,1250,1030	υC–N

FTIR Analysis

FTIR spectroscopy is a powerful analytical technique widely employed for both qualitative and quantitative analysis, relying on the principle of molecular vibrational transitions [28, 29]. This method is particularly effective for identifying functional groups in organic and inorganic compounds, as different functional groups exhibit characteristic absorption patterns within specific frequency ranges [30]. Additionally, the polarity of the solvent can significantly influence the FTIR spectra of compounds due to interactions between the solvent and the analyte, a phenomenon referred to as the solvent effect [31].

In the present study, triallyl isocyanurate was investigated using FTIR spectroscopy in various solvents, including water, tetrahydrofuran, dimethyl sulfoxide, and acetonitrile. The obtained spectral data are illustrated in Fig. 2.

In the FTIR spectra (Fig. 2, Table 1), the absorption peak –C=C– and –C=O for triallyl isocyanurate is located at 1641 and 1720 cm^{-1}, respectively [32, 33]. Also clear absorption bands around 1720, 1635, 1632 cm^{-1}, shown in Fig. 1, corresponds to the carbonyl stretching vibration (C=O). The isocyanurate ring, the product of trimerization of isocyanate, can usually be identified by a C–N stretch band in the region of 1300–1460 cm^{-1} [34, 35]. Stretching vibrations of the C–H group are observed in the region of 2900–3700 cm^{-1}.

It should be noted that the effect of the solvent is clearly visible in all experimental spectra (Fig. 2). Thus, for the solvent water, there is a wide absorption band at 3000–3500 cm^{-1}, which corresponds to vibrations of the OH groups of water [36]. In all experimental spectra, the influence of the solvent is decisive, while in theoretical spectra it only leads to a change in the intensity of individual peaks.

The Highest Occupied Molecular Orbital and the Lowest Unoccupied Molecular Orbital Analysis

The energies of electronic levels are critical parameters that characterize materials and are widely utilized across various scientific and industrial fields. Of particular importance are the energies of ionized levels, which include the highest occupied molecular orbital and the lowest unoccupied molecular orbital. These levels represent the energy states available for excess holes and excess electrons, respectively, and serve as key indicators of a material's electronic properties [37].

The energy separation between the HOMO and LUMO, often referred to as the HOMO–LUMO gap, is a fundamental parameter used to assess kinetic and chemical stability [38–41]. A larger HOMO–LUMO gap typically indicates higher kinetic stability and lower chemical reactivity. This is because a significant energy difference makes it energetically unfavorable to either add electrons to the high-lying LUMO or remove electrons from the low-lying HOMO, thereby hindering the formation of an activated complex and reducing reactivity [38, 42].

A graphical illustration of the HOMO–LUMO concept is provided in Fig. S1, while the correspond-

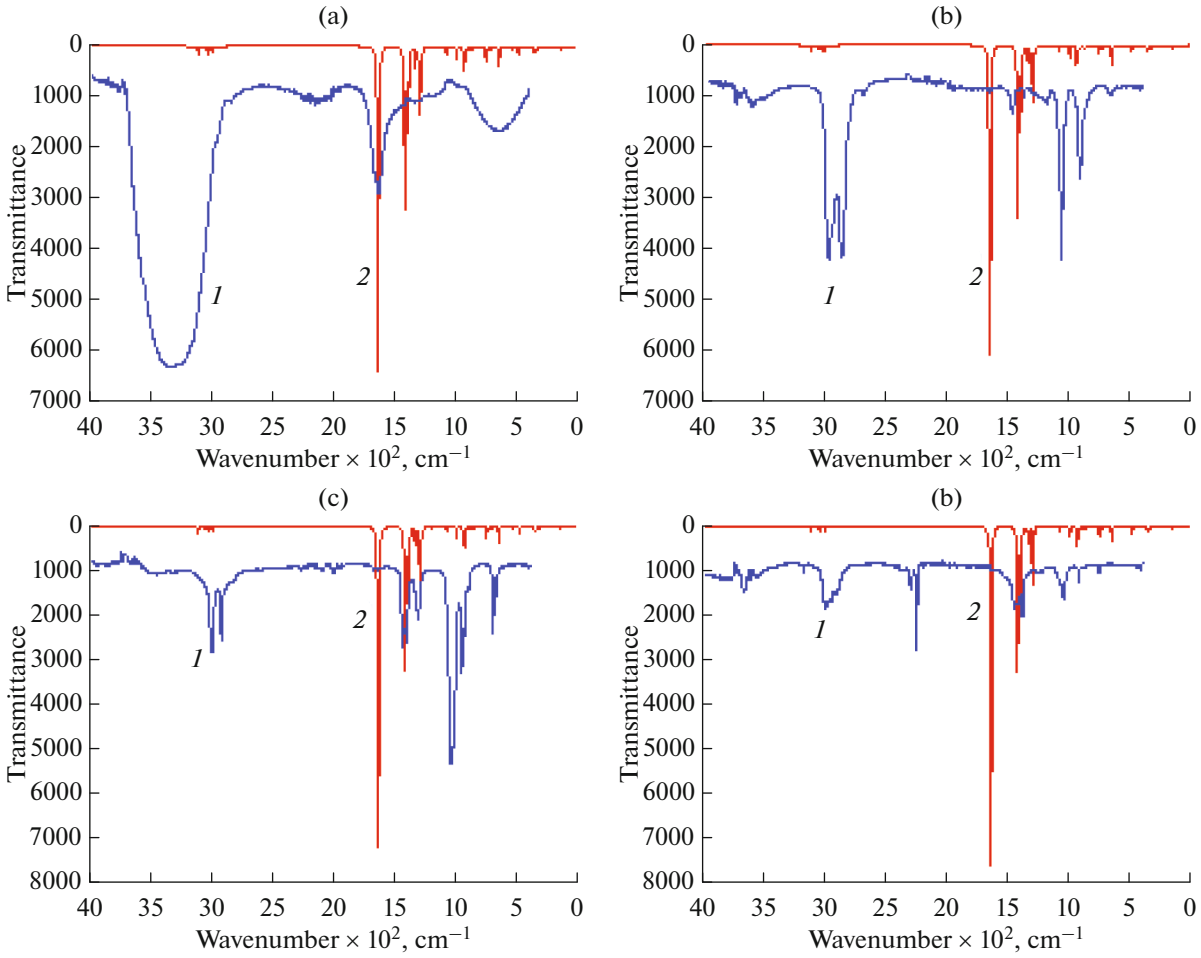

Fig. 2. FTIR spectra of TAIC: (1) experimental, (2) theoretical: (a) water, (b) THF, (c) DMSO and (d) ACN.

ing analysis data, including HOMO and LUMO energy values, is summarized in Table 2.

Based on the data provided in Table 2, the energy gap (HOMO–LUMO gap) values for triallyl isocyanurate in the studied solvents range from 4.8229 eV (for THF) to 4.8366 eV (for water). Overall, the parameters analyzed for triallyl isocyanurate exhibit comparable values across all solvents. Specifically, the electronegativity (χ) values are as follows: 7.2483 for water, 7.2494 for THF, 7.2483 for DMSO, and 7.2484 for ACN. The chemical hardness (η) values reach their maximum in water and their minimum in THF. A similar trend is observed for the electrophilicity index (N) and the chemical potential (μ), indicating consistent behavior across the solvents.

Dipole moment μ (D), Polarizability α (e.s.u), and first order hyperpolarizability β (e.s.u) of TAIC in different solvents was calculated (Table 3).

According to the data given in Table 3, these characteristics have different meanings for TAIC in different solvents. Thus, the value of μ(D) for Water, THF, DMSO, ACN is 0.0778, 0.1287, 0.1317, 0.0158, respectively. The values of βtot (e.s.u) Water, THF, DMSO, ACN are 12.621×10^{-30}, 12.5368×10^{-30}, 12.5943×10^{-30}, 12.582×10^{-30}, respectively. The α (e.s.u) values of Water, THF, DMSO, ACN are 33.7412×10^{-23}, 34.8353×10^{-23}, 34.0520×10^{-23}, 33.509×10^{-23}, respectively.

Ultraviolet-Visible Spectroscopy Analysis

Ultraviolet-visible spectroscopy is a versatile analytical technique widely employed for qualitative and quantitative analysis, structural determination, and real-time monitoring of reactions across diverse media [43]. This method relies on the interaction of a light source with the sample, which can be analyzed through absorption, transmission, or reflection within the UV-visible spectral range [44–46].

In this study, triallyl isocyanurate was also investigated using UV-vis spectroscopy in various solvents, including water, tetrahydrofuran, dimethyl sulfoxide, and acetonitrile. The results are presented in Fig. 4. As shown in the figure, the solvents do not significantly

alter the position of the absorption peak for triallyl isocyanurate but do influence its intensity.

According to the data presented in Table 4, in the UV-vis spectra, the TAIC peak is in the range from 206.07 to 206.38 nm, depending on the solvent. The *f* values also have comparable values: from 0.0006–0.0007 eV. Eex values range from 6.0074 to 6.0167 eV depending on the solvent used (within the test substances).

Non-Covalent Interaction Reduced Density Gradient Analysis

Non-covalent interactions within molecular clusters were analyzed using NCI-RDG methods. These techniques are highly effective for identifying and visualizing weak interactions, such as hydrogen bonding, van der Waals forces, and steric (repulsive) effects, through distinct color-coded or numbered representations. The NCI index serves as a robust indicator of non-covalent interactions and is closely associated with the reduced density gradient. The RDG is a dimensionless parameter derived from the electron density and its first derivative, as described by the following formula [47]:

$$\mathrm{RDG}(r) = \frac{1}{2\left(3\pi^2\right)^{1/3}} \frac{|\nabla \rho(r)|}{\rho(r)^{4/3}}.$$

The electron density peaks, characterized by the parameter $\mathrm{sign}(\lambda_2)\rho$ (where λ_2 is the second eigenvalue of the Hessian matrix), provide critical insights into the nature and strength of molecular interactions

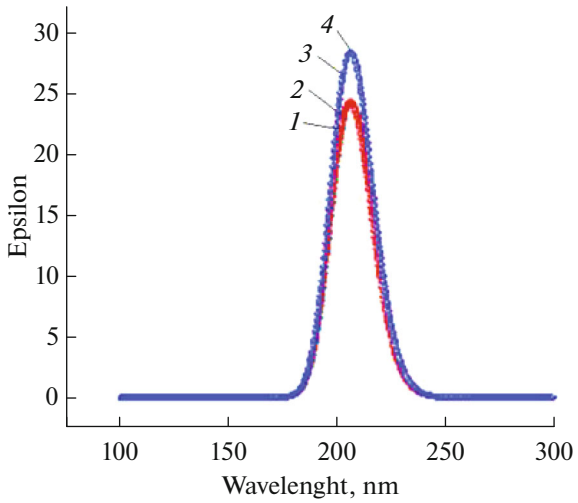

Fig. 3. UV-Vis spectra of TAIC: (*1*) water, (*2*) THF, (*3*) DMSO and (*4*) ACN.

when analyzed in relation to the reduced density gradient. The value of $\mathrm{sign}(\lambda_2)\rho$ is particularly significant in determining the type of interaction: $\mathrm{sign}(\lambda_2)\rho > 0$ indicates repulsive interactions (non-bonded), while $\mathrm{sign}(\lambda_2)\rho < 0$ signifies attractive interactions (bonded).

The NCI isosurface and RDG scatter maps of triallyl isocyanurate are presented in Fig. 5. On the left side of Fig. 5, the color-coded regions reveal the nature of interactions: blue (number 1) represents hydrogen bonding, green (number 2) corresponds to van der Waals interactions, and red (number 3) indi-

Table 2. Electronic parameters obtained from HOMO and LUMO energies for TAIC in different solvents

Parameter	W	THF	DMSO	ACN
E_{LUMO}	–4.8300	–4.8379	–4.8306	–4.8311
E_{HOMO}	–9.6666	–9.6609	–9.6660	–9.6658
ΔE	4.8366	4.8229	4.8355	4.8346
IP	9.6666	9.6609	9.6660	9.6658
EA	4.8300	4.8379	4.8306	4.8311
χ	7.2483	7.2494	7.2483	7.2484
μ	–7.2483	–7.2494	–7.2483	–7.2484
η	2.4183	2.4115	2.4177	2.4173
ζ	0.4135	0.4147	0.4136	0.4137
ω	10.8627	10.8966	10.8651	10.8673
ΔN_{max}	2.9973	3.0062	2.9980	2.9985
N	0.0921	0.0918	0.0920	0.0920
$\sigma_{\circ}$	0.2068	0.2073	0.2068	0.2068

Table 3. Computed values of dipole moment μ (D), Polarizability α (e.s.u), and first order hyperpolarizability β (e.s.u) of TAIC in different solvents

Parameters	W	THF	DMSO	ACN
μ_x	0.0382	0.0248	0.0275	0.0529
μ_y	−0.0331	−0.1263	−0.1288	−0.0126
μ_z	0.0592	0.0009	0.0009	0.0330
μ	0.0778	0.1287	0.1317	0.0158
α_{xx}	34.9318	35.5093	35.0011	34.6671
α_{xy}	−1.7131	−1.9192	−1.8613	−1.7046
α_{yy}	40.7728	42.0843	41.5484	40.4649
α_{xz}	−0.6690	0.7110	−0.6911	−0.6683
α_{yz}	−1.2995	−1.6098	−1.500	−1.1513
α_{zz}	25.5190	27.9243	26.7202	25.3708
a, a.u	227.6734	228.0393	228.9663	226.0522
a, e.s.u	33.7412×10^{-23}	34.8353×10^{-23}	34.0520×10^{-23}	33.509×10^{-23}
Δ*a*, a.u	418.5024	468.6206	419.5905	414.8205
Δ*a*, e.s.u	61.9547×10^{-23}	63.0011×10^{-23}	62.4548×10^{-23}	61.4946×10^{-23}
β_{xxx}	144.0021	150.0249	149.5287	132.1206
β_{xxy}	−105.2412	−107.9100	−107.6709	−104.4225
β_{xyy}	−75.4397	−77.4143	−76.8347	−74.9245
β_{yyy}	32.0659	32.7465	32.4220	31.9073
β_{zxx}	0.5805	0.5681	0.6765	0.5663
β_{xyz}	−0.2032	−0.4037	−0.3034	−0.1716
β_{zyy}	0.4462	0.6436	0.5453	0.3136
β_{xzz}	−14.8846	−15.9815	−15.6604	−13.9175
β_{yzz}	−22.3943	−23.7524	−23.1896	−21.7368
β_{zzz}	−0.0547	−0.0851	−0.0618	−0.0247
β_{tot}, a.u	156.4229	160.6315	160.2947	144.0646
β_{tot}, e.s.u	12.621×10^{-30}	12.5368×10^{-30}	12.5943×10^{-30}	12.582×10^{-30}

cates strong repulsion (steric effects). Similarly, on the right side of Fig. 5, the color scheme is consistent, with blue (number 1) denoting hydrogen bonding, green (number 2) representing van der Waals forces, and red (number 3) highlighting steric repulsion.

The presence of blue discs (number 1) between O–H···O, O–H···N, and N–H···O bonds in the molecular clusters confirms hydrogen bonding, aligning with the results obtained from AIM (Atoms in Molecules) analysis. In the case of TAIC interacting with THF, regions with red and green coloring dominate, indicating a mix of steric repulsion and van der Waals interactions. Conversely, for TAIC with DMSO or ACN, the maps show predominantly green regions, suggesting a stronger presence of van der Waals interactions.

Electron Localization Function and Localized Orbital Locator Topological Surface Analyses

To gain deeper insights into covalent bonding within molecular interactions, we conducted Electron Localization Function and Localized Orbital Locator topological surface analyses. These methods are

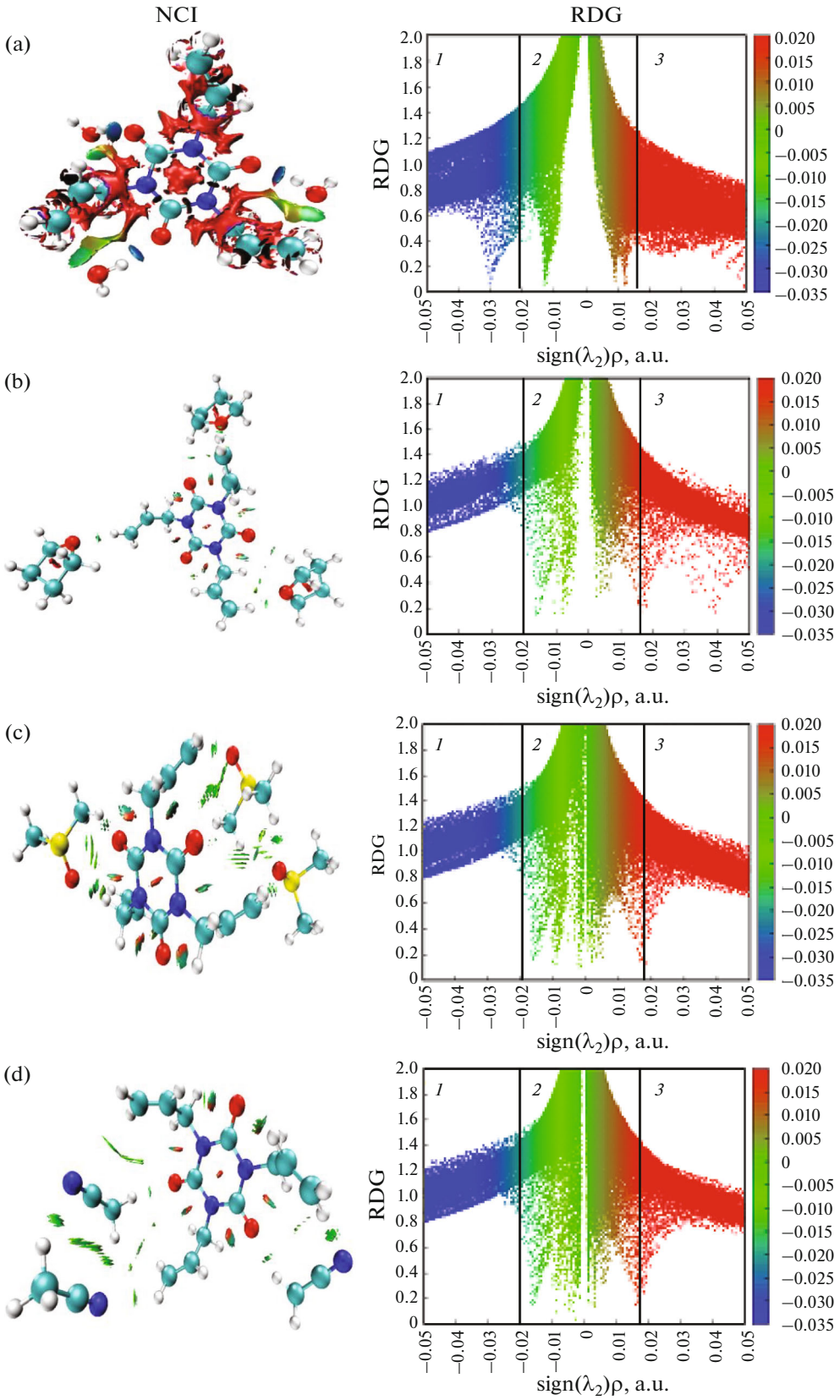

Fig. 4. NCI-RDG analysis of TAIC with solvents: (a) water, (b) THF, (c) DMSO and (d) ACN.

Table 4. Absorption data for TAIC in different solvents

Medium	Electronic transitions	E_{ex}, eV	λ, nm	f, eV	Transition probability, %
Water	S0 → S3	6.0074	206.38	0.0006	H-5 → L+1(9) H-4 → L (14) H-1 → L (19) H → L+1 (53)
THF	S0 → S3	6.0167	206.07	0.0006	H-5 → L+1(11) H-4 → L (17) H-1 → L (17) H → L+1 (49)
DMSO	S0 → S3	6.0109	206.27	0.0007	H-5 → L+1(11) H-4 → L (17) H-1 → L (17) H → L+1 (50)
ACN	S0 → S3	6.0112	206.25	0.0007	H-5 → L+1(11) H-4 → L (17) H-1 → L (17) H → L+1 (50)

designed to identify regions with a high probability of locating electron pairs, providing valuable information about electron distribution and bonding characteristics [48–50]. While ELF and LOL are conceptually similar, they differ in their specific applications: ELF generalizes to spin-polarized systems and reflects electron localization relative to the Fermi hole, whereas LOL provides a more precise representation by focusing on the true kinetic energy term.

The ELF and LOL color maps for the studied molecular interactions are displayed in Figs. S2 and S3, respectively. The ELF values range from 0.0 to 1.0, while the LOL values range from 0.0 to 0.8. Analysis of the color maps reveals distinct patterns:

• In the ELF map, regions around hydrogen atoms appear in red, indicating high electron localization, while blue regions around carbon atoms suggest a delocalized electron cloud.

• In the LOL map, the center of hydrogen atoms appears white, signifying that the electron density exceeds the upper limit of the color scale (0.80). Nitrogen and several carbon nuclei display circular blue regions, representing areas of electron loss between the valence and inner shells.

• Red circles highlight the most significant covalent regions, particularly between carbon- carbon and carbon-nitrogen atoms.

The color gradients in both ELF and LOL maps confirm the presence of bonding and non-bonding electrons. Specifically, the red regions around hydrogen atoms indicate the presence of both bonding and non-bonding electrons at their maximum values.

Atoms in Molecules Analysis

Numerous theoretical studies [48–51] have demonstrated that Atoms in Molecules analysis, introduced by Bader and his collaborators [52–54], is one of the most effective tools for characterizing weak interactions, such as intra- and intermolecular hydrogen bonding, in various molecular systems. According to this theory, bond critical points (BCPs) emerge between atoms due to the spatial concentration of electrons. At these points, the gradient of the electron density vanishes: $\nabla^2\rho_{BCP} = 0$. BCPs are crucial for identifying and characterizing chemical bonds, including hydrogen bonds. While Popelier and Koch [55] proposed several topological parameters to describe hydrogen bonding, the most commonly used are the electron density (ρ_{BCP}) and the Laplacian of electron density ($\nabla^2\rho_{BCP}$) at the BCP. For hydrogen bonding to be confirmed, the values of ρ_{BCP} should fall within the range of 0.0033–0.168 a.u., and $\nabla^2\rho_{BCP}$ should be between 0.024–0.139 a.u. [56].

Rozas and colleagues [57–59] further classified hydrogen bonding interactions into three categories based on the Laplacian of electron density and the energy density at the BCP:

(1) Strong hydrogen bonds: Characterized by $\nabla^2\rho(r) < 0$ and $H_{BCP} < 0$, indicating a covalent nature.

(2) Medium hydrogen bonds: Defined by $\nabla^2\rho(r) > 0$ and $H_{BCP} < 0$, suggesting a partially covalent character.

(3) Weak hydrogen bonds: Identified by $\nabla^2\rho(r) > 0$ and $H_{BCP} > 0$, primarily electrostatic in nature.

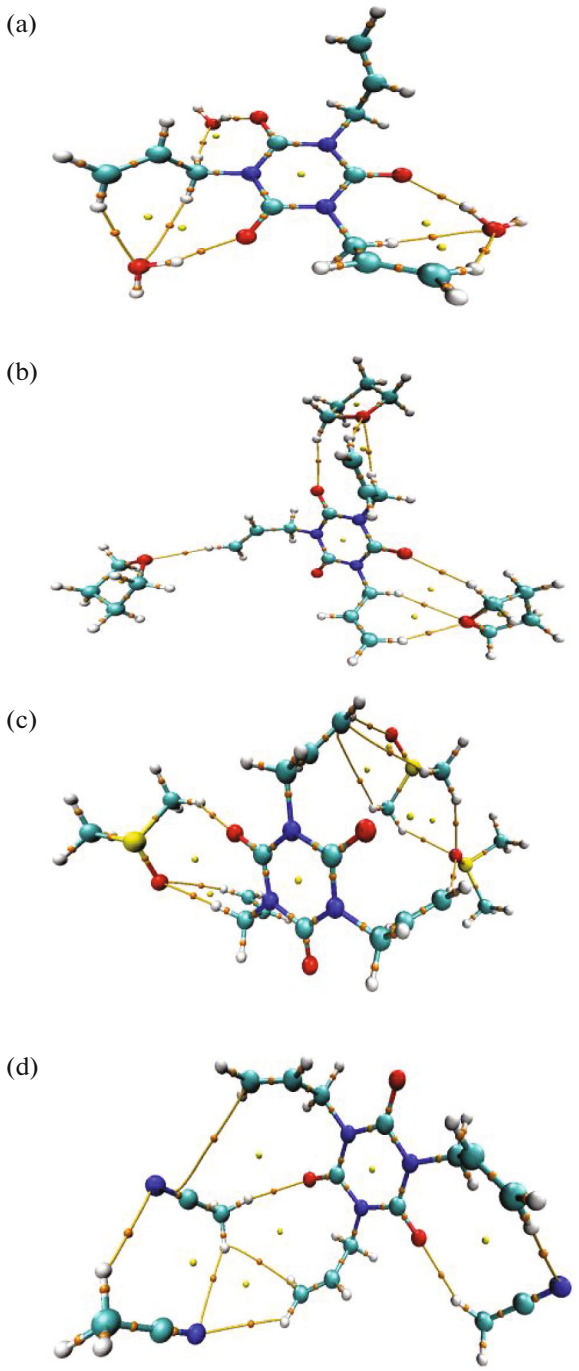

Fig. 5. AIM analysis of TAIC with solvents.

In Fig. 5, the molecular diagram of triallyl isocyanurate with solvents is illustrated. The BCPs are marked by orange dots, ring critical points (RCPs) by yellow dots, and cage critical points (CCPs) by green dots. Table 5 provides detailed topological parameters at the BCPs, including the electron density $\rho(r)$, the Laplacian of electron density $\nabla^2\rho(r)$, the Lagrangian kinetic energy $G(r)$, the potential energy $V(r)$, the energy density $H(r)$, and the hydrogen bond energy E_{HB}. The

Table 5. Topological parameters obtained from AIM analysis for TAIC + W, TAIC + THF, TAIC + DMSO and TAIC + ACN

Contact type	ρ_{BCPs}	$\nabla^2\rho_{BCPs}$	H_{BCPs}	E_{HB}
TAIC + W				
O34···H31	0.0097	0.0334	0.0007	−2.1648
H40···O3	0.0227	0.0745	0.0005	−5.4906
O34···H21	0.0063	0.0257	0.0011	−1.2863
H32···O36	0.0096	0.0327	0.0007	−2.1021
H23···O36	0.0072	0.0284	0.0011	−1.5060
H41···O2	0.0233	0.0759	0.0005	−5.6161
H22···O38	0.0085	0.0289	0.0008	−1,7570
O1···H42	0.0229	0.0727	0.0002	−5.5533
TAIC + THF				
H32···O71	0.0081	0.0277	0.0007	−1.6942
O71···H23	0.0067	0.0238	0.0008	−1.3491
O46···H30	0.0106	0.0326	0.0003	−2,3217
H51···O2	0.0081	0.0296	0.0009	−1,7256
O1···H63	0.0080	0.0293	0.0009	−1.6942
H20···O72	0.0072	0.0251	0.0007	−1.4746
H28···O72	0.0078	0.0269	0.0007	−1.6315
TAIC + DMSO				
H20···O37	0.0104	0.0327	0.0004	−2.2590
O37···H28	0.0096	0.0318	0.0006	−2.1021
H33···O36	0.0081	0.0277	0.0006	−1.7256
O1···H43	0.0093	0.0356	0.0011	−2.0707
O36···H45	0.0104	0.0334	0.0005	−2.2903
O36···H51	0.0087	0.0304	0.0007	−1.8825
H30···O34	0.0090	0.0297	0.0007	−1.8511
TAIC + ACN				
N48···H33	0.0043	0.0149	0.0008	−0.6588
N48···H40	0.0047	0.0157	0.0007	−0.7216
H43···N50	0.0080	0.0265	0.0010	−1.3805
H36···O2	0.0097	0.0361	0.0010	−2.1648
N46···H28	0.0060	0.0193	0.0008	−0.9726
H39···O3	0.0088	0.0306	0.0007	−1.8825

ρ—the electron density (a.u.), $\nabla^2\rho$—the Laplacian of electron density (a.u.), H—the energy density (a.u.) and E_{HB}—H–bond energy (kcal/mol) at the bond critical points (BCPs).

hydrogen bond energy was calculated using the following relationship [60–67]:

$$E_{HB} = -V(r_{CP})627.5/2,$$

where $V(r_{CP}) = 1/4\nabla^2\rho_{BCP} - 2G(r_{CP})$ is potential energy density in the BCPs.

The values of electron density (ρ) and electron density Laplacian ($\nabla^2\rho$) at BCPs for triallyl isocyanurate interacting with water, THF, DMSO, and ACN fall within the following ranges:

• Water: ρ = 0.0085–0.0233 a.u., $\nabla^2\rho$ = 0.0067–0.0106 a.u.

• THF: ρ = 0.0081–0.0104 a.u., $\nabla^2\rho$ = 0.0043–0.0097 a.u.

• DMSO: ρ = 0.0081–0.0104 a.u., $\nabla^2\rho$ = 0.0043–0.0097 a.u.

• ACN: ρ = 0.0043–0.0097 a.u., $\nabla^2\rho$ = 0.0043–0.0097 a.u.

These values, illustrated in Fig. 6 and detailed in Table 5, lie within the established range for hydrogen bonding. Additionally, the bond lengths between the interacting atoms are shorter than the sum of their van der Waals radii, further confirming the presence of hydrogen bonds in these systems. The calculated hydrogen bond energies range from –0.97 to –5.62 kcal/mol, indicating weak to moderate hydrogen bonding interactions.

CONCLUSIONS

For the first time, a comprehensive (theoretical and experimental) study of triallyl isocyanurate was carried out, and the effect of the solvent on its energy structure was assessed. Data were obtained from Experimental and Theoretical Vibrational Spectroscopy, MEP, TD-DFT study, AIM, NCI-RDG, ELF-LOL, HOMO–LUMO analyses. It has been shown that the solvent plays a decisive role in the analysis by FTIR spectroscopy. The values of electron density and electron density Laplacian in BCPs of TAIC with water, THF, DMSO and ACN are in the range of 0.0085–0.0233 a.u., 0.0067–0.0106 a.u., 0.0081–0.0104 a.u. and 0.0043–0.0097 a.u., respectively. The energies of such hydrogen bonds vary between –0.97 and –5.62 kcal/mol. The color shades of ELF and LOL maps confirm the presence of bonding and non-bonding electrons, where the red color around hydrogen atoms shows the presence of bonding and non-bonding electrons with maximum value. According to RDG analysis, the interaction of TAIC with THF is characterized by regions with red and green coloring, while for TAIC with DMSO or ACN, more green regions are observed. The color shades of ELF and LOL maps confirm the presence of bonding and non-bonding electrons, where the red color around hydrogen atoms shows the presence of bonding and non-bonding electrons with maximum value.

In summary, the study provides a detailed understanding of the solvent-dependent electronic and structural properties of TAIC, highlighting the significance of solvent effects in molecular interactions and spectroscopic analysis.

SUPPLEMENTARY INFORMATION

The online version contains supplementary material available at https://doi.org/10.1134/S1990793125701520.

ACKNOWLEDGMENTS

Ongoing Research Funding program, (ORF—2025–61), King Saud University, Riyadh, Saudi Arabia. The authors thank University of Bingöl for the server and University of Bitlis Eren for the Gaussian 09W software. This study was also partially carried out within the budget plan no. FWES-2026-0011 for the Institute of Chemistry and Chemical Technology, Siberian Branch of the Russian Academy of Sciences.

FUNDING

The theoretical study was supported by the Ongoing Research Funding program, (ORF—2025–61), King Saud University, Riyadh, Saudi Arabia. This study was also partially carried out within the budget plan no. FWES-2026-0011 for the Institute of Chemistry and Chemical Technology, Siberian Branch of the Russian Academy of Sciences.

CONFLICT OF INTEREST

The authors of this work declare that they have no conflicts of interest.

REFERENCES

1. B. Merillas, J. Martín-de León, F. Villafañe, and M. Á. Rodríguez-Pérez, Nanomaterials **12**, 1522 (2022).
2. M. Riahinezhad, M. Hallman, and J. F. Masson, Buildings **11**, 299 (2021).
3. S. Yamane, H. Shinzawa, S. Ata, Y. Suzuki, A. Nishizawa, and J. Mizukado, Vib. Spectrosc. **98**, 30 (2018).
4. N. Nagasawa, A. Kaneda, S. Kanazawa, T. Yagi, H. Mitomo, F. Yoshii, and M. Tamada, Nucl. Instrum. Methods Phys. Res., Sect. B **236**, 611 (2005).
5. P. Rytlewski, M. Stepczyńska, U. Gohs, R. Malinowski, B. Budner, and M. Żenkiewicz, Ind. Crops Prod. **112**, 716 (2018).
6. J. K. Gillham and A. F. Lewis, Nature **195**, 1199 (1962).
7. R. W. Roth and R. F. Church, J. Polym. Sci. **55**, 41 (1961).
8. J. K. Gillham and C. C. Mentzer, J. Appl. Polym. Sci. **17**, 1143 (1973).
9. X. Chen, X. Huang, T.-Y. Shi, J.-X. Wang, X.-R. Yuan, H. Huang, J. Wang, R. He, and X.-F. Yu, ACS Omega **7**, 14952 (2022).

10. H. Zhao, J. Chen, H. Zhang, Y. Shang, X. Wang, B. Han, and Z. Li, RSC Adv. **7**, 37095 (2017).
11. C.-M. Zhang, F. Li, X.-Q. Zhu, and J.-G. Yu, Molecules **27**, 3107 (2022).
12. National Center for Biotechnology Information (2025). PubChem Compound Summary for CID 13931, Triallyl isocyanurate. Retrieved October 25, 2025. https://pubchem.ncbi.nlm.nih.gov/compound/Triallyl-isocyanurate.
13. P. Ho and G. Wu, Biomater., Artif. Cells, Artif. Organs **15**, 199 (1987).
14. J. Ma, L. Chen, and B. He, J. Appl. Polym. Sci. **61**, 2029 (1996).
15. F. Akman, A. S. Kazachenko, and N. Issaoui, Polym. Sci., Ser. B **64**, 765 (2022).
16. N. Kosar, S. Noreen, K. Ayub, M. Imran, and T. Mahmood, Inorg. Chem. Commun. **157**, 111328 (2023).
17. N. Kosar, H. Sajid, M. Z. Ahmed, K. Ayub, and T. Mahmood, Comput. Theor. Chem. **1226**, 114226 (2023).
18. N. Kosar, L. Zari, K. Ayub, M. A. Gilani, and T. Mahmood, Phys. Scr. **98**, 065909 (2023).
19. J. Yaqoob, S. Tabassum, H. AlMohamadi, T. Mahmood, K. Ayub, A. L. Khan, M. Yasin, and M. A. Gilani, Phys. Scr. **98**, 095516 (2023).
20. A. Nisar, S. Tabassum, K. Ayub, T. Mahmood, H. AlMohamadi, A. L. Khan, M. Yasin, R. Nawaz, and M. A. Gilani, Phys. Chem. Chem. Phys. **25**, 20430 (2023).
21. N. Kosar, S. Wajid, K. Ayub, and T. Mahmood, Optik **276**, 170660 (2023).
22. M. J. Frisch et al., Gaussian 09, Revision C.01 (Gaussian, Inc., Wallingford, CT, 2009).
23. GaussView, Version 5.0 (Gaussian, Inc., Pittsburgh, PA, 2000–2003).
24. A. D. Becke, Phys. Rev. A **38**, 3098 (1988).
25. C. Lee, W. Yang, and R. G. Parr, Phys. Rev. B **37**, 785 (1988).
26. J. Zhang and M. Dolg, Phys. Chem. Chem. Phys. **17**, 24173 (2015).
27. T. Lu and F. Chen, J. Comput. Chem. **33**, 580 (2012).
28. A. S. Kazachenko, F. N. Tomilin, A. A. Pozdnyakova, N. Y. Vasilyeva, Y. N. Malyar, S. A. Kuznetsova, and P. V. Avramov, Chem. Pap. **74**, 4103 (2020).
29. H. Henschel, A. T. Andersson, W. Jespers, M. Mehdi Ghahremanpour, and D. van der Spoel, J. Chem. Theory Comput. **16**, 3307 (2020).
30. I. Carnimeo, C. Puzzarini, N. Tasinato, P. Stoppa, A. P. Charmet, M. Biczysko, C. Cappelli, and V. Barone, J. Chem. Phys. **139**, 074310 (2013).
31. C. Parlak and P. Ramasami, SN Appl. Sci. **2**, 1148 (2020).
32. X. Yu, Z. Fang, Y. Qin, D. Lu, Q. Liu, L. Luo, Z. Lin, and K. Wang, J. Polym. Res. **28**, 272 (2021).
33. S. Muroga, Y. Takahashi, Y. Hikima, S. Ata, M. Ohshima, T. Okazaki, and K. Hata, Polym. Test. **93**, 106993 (2021).
34. B. Raffel and C. J. Loevenich, J. Cell. Plast. **42**, 17 (2006).
35. J. Reignier, F. Méchin, and A. Sarbu, Polym. Test. **93**, 106972 (2021).
36. F. Cheng, Q. Cao, Y. Guan, H. Cheng, X. Wang, and J. D. Miller, Int. J. Miner. Process. **122**, 36 (2013).
37. J. Sworakowski, Synth. Met. **235**, 125 (2018).
38. J. Aihara, J. Phys. Chem. A **103**, 7487 (1999).
39. D. E. Manolopoulos, J. C. May, and S. E. Down, Chem. Phys. Lett. **181**, 105 (1991).
40. A. S. Kazachenko, F. Akman, N. Y. Vasilieva, N. Issaoui, Y. N. Malyar, A. A. Kondrasenko, V. S. Borovkova, A. V. Miroshnikova, A. S. Kazachenko, O. Al-Dossary, M. J. Wojcik, Y. D. Berezhnaya, and E. V. Elsuf'ev, Int. J. Mol. Sci. **23**, 1602 (2022).
41. A. S. Kazachenko, E. Tanış, F. Akman, M. Medimagh, N. Issaoui, O. Al-Dossary, L. G. Bousiakou, A. S. Kazachenko, D. Zimonin, and A. M. Skripnikov, Molecules **27** (22), 7864 (2022).
42. S. Kaviani, M. Izadyar, and M. R. Housaindokht, Polyhedron **117**, 623 (2016).
43. J. C. Lindon, G. E. Tranter, and D. Koppenaal, *Encyclopedia of Spectroscopy and Spectrometry* (Elsevier, 2016).
44. Y. Guo, C. Liu, R. Ye, and Q. Duan, Appl. Sci. **10** (19), 6874 (2020).
45. M. A. Lutoshkin, A. I. Petrov, Y. N. Malyar, and A. S. Kazachenko, Inorg. Chem. **60**, 3291 (2021).
46. M. A. Lutoshkin and A. S. Kazachenko, J. Comput. Methods Sci. Eng. **17**, 851 (2017).
47. B. Silvi and A. Savin, Nature **371**, 683 (1994).
48. A. S. Kazachenko, N. Issaoui, A. Sagaama, Y. N. Malyar, O. Al-Dossary, L. G. Bousiakou, A. S. Kazachenko, A. V. Miroshnokova, and Z. Xiang, J. King Saud Univ., Sci. **34**, 102350 (2022).
49. A. Jumabaev, U. Holikulov, H. Hushvaktov, N. Issaoui, and A. Absanov, J. Mol. Liq. **377**, 121552 (2023).
50. M. Khodiev, U. Holikulov, A. Jumabaev, N. Issaoui, N. Lvovich, O. M. Al-Dossary, and L. G. Bousiakoug, J. Mol. Liq. **382**, 121960 (2023).
51. A. Kazachenko, F. Akman, M. Medimagh, N. Issaoui, N. Vasilieva, Y. N. Malyar, I. G. Sudakova, A. Karacharov, A. Miroshnikova, and O. M. Al-Dossary, ACS Omega **6**, 22603 (2021).
52. R. F. W. Bader, Acc. Chem. Res. **18**, 9 (1985).
53. R. F. W. Bader, *Atoms in Molecules: A Quantum Theory* (Oxford University Press, Oxford, 1990).
54. R. F. W. Bader, J. Chem. Phys. **91**, 6989 (1989).
55. U. Koch and P. L. A. Popelier, J. Phys. Chem. **99**, 9747 (1995).
56. T. H. Tang, E. Deretey, S. J. Knak Jensen, and I. G. Csizmadia, Eur. Phys. J. D **37**, 217 (2006).
57. I. Rozas, I. Alkorta, and J. Elguero, J. Am. Chem. Soc. **122**, 11154 (2000).
58. F. Cortés-Guzmán, J. I. Rodríguez, and J. S. M. Anderson, in *Advances in Quantum Chemical Topology Beyond QTAIM*, Ed. by J. I. Rodríguez, F. Cortés-Guzmán, and J. S. M. Anderson (Elsevier, 2023), p. 1.
59. X. Nie, Y. Yang, T. Xu, S. R. Kirk, and S. Jenkins, in *Advances in Quantum Chemical Topology Beyond QTAIM*, Ed. by J. I. Rodríguez, F. Cortés-Guzmán, and J. S. M. Anderson (Elsevier, 2023), p. 111.

60. E. Espinosa, E. Molins, and C. Lecomte, Chem. Phys. Lett. **285**, 170 (1998).

61. J. Pilmé, E. Renault, F. Bassal, M. Amaouch, G. Montavon, and N. Galland, J. Chem. Theory Comput. **10**, 4830 (2014).

62. S. Shahbazian, in *Advances in Quantum Chemical Topology Beyond QTAIM*, Ed. by J. I. Rodríguez, F. Cortés-Guzmán, and J. S. M. Anderson (Elsevier, 2023), p. 73.

63. F. Heidar-Zadeh, P. W. Ayers, T. Verstraelen, I. Vinogradov, E. Vöhringer-Martinez, and P. Bultinck, J. Phys. Chem. A **122**, 4219 (2018).

64. I. Alkorta and J. Elguero, Chem. Phys. Lett. **417**, 367 (2006).

65. J. Cioslowski and J. Karwowski, in *Fundamentals of Molecular Similarity*, Ed. by R. Carbó-Dorca, X. Gironés, and P. G. Mezey (Springer US, Boston, MA, 2001), p. 101.

66. D. J. Cole, J. Z. Vilseck, J. Tirado-Rives, M. C. Payne, and W. L. Jorgensen, J. Chem. Theory Comput. **12**, 2312 (2016).

67. D. Vega and D. Almeida, J. Comput. Methods Sci. Eng. **14**, 131 (2014).